MODELING LONGSHORE CURRENTS FOR FIELD SITUATIONS

by

Seetharama R. Vemulakonda[1], James R. Houston[2],
and H. Lee Butler[3], Members ASCE

Abstract

There is a growing need for generalized numerical models for long-
shore currents and nearshore circulation that solve the complete equa-
tions of motion, are flexible in the formulations chosen for various
terms, and can be applied to field situations at a reasonable cost. The
development and application of one such model is described in this
paper. The model was first tested by comparing its results to known
analytic solutions and experimental data. There was good agreement. It
was next applied to a field situation near Oregon Inlet, North Carolina.
The results appeared to be reasonable and the computational costs were
modest.

Introduction

Over the last two decades, a considerable amount of literature has
been published on the computation of longshore currents and nearshore
circulation due to the action of breaking waves. However, most of this
literature (for example, 2, 6, 8, 10, 12) has been devoted to idealized
situations such as plane beaches and periodic bathymetries. Often the
analytical and numerical models used have been limited in scope. The
limitations include assuming a steady state, using a linear friction,
neglecting advection and/or eddy viscosity terms, etc. The development
of generalized numerical models (5, 13) that can handle more complex
situations is relatively recent. As of now (1982), very little work has
been reported on the application of numerical current models to field
situations at a reasonable cost. In view of the increasing tendency of
the coastal engineering profession to employ numerical models for sedi-
ment transport in the nearshore region, there is a pressing need for
generalized longshore current models. In this paper, the development
and application of one such model is described.

---

[1] Research Division, Coastal Engineering Research Center, Fort Belvoir,
Virginia 22060; formerly, Wave Dynamics Division, U. S. Army Engineer
Waterways Experiment Station, Vicksburg, MS 39180.

[2,3] Wave Dynamics Division, U. S. Army Engineer Waterways Experiment
Station, P. O. Box 631, Vicksburg, Mississippi 39180, U.S.A.

Equations of Motion

The governing equations for the problem under consideration are obtained from the general equations of conservation of mass and momentum, after averaging over time (one wave period) and depth. They are expressed in terms of the mean horizontal velocities U , V and the mean free surface displacement $\bar{\eta}$ as follows (refer to Fig. 1):

Momentum

$$\frac{\partial U}{\partial t} + U\frac{\partial U}{\partial x} + V\frac{\partial U}{\partial y} + g\frac{\partial \bar{\eta}}{\partial x} + \frac{1}{\rho d}\ \tau_{bx} + \frac{1}{\rho d}\ (\frac{\partial S_{xx}}{\partial x} + \frac{\partial S_{xy}}{\partial y}) - \frac{1}{\rho}\frac{\partial \tau_{xy}}{\partial y} = 0 \quad (1)$$

$$\frac{\partial V}{\partial t} + U\frac{\partial V}{\partial x} + V\frac{\partial V}{\partial y} + g\frac{\partial \bar{\eta}}{\partial y} + \frac{1}{\rho d}\ \tau_{by} + \frac{1}{\rho d}\ (\frac{\partial S_{xy}}{\partial x} + \frac{\partial S_{yy}}{\partial y}) - \frac{1}{\rho}\frac{\partial \tau_{xy}}{\partial x} = 0 \quad (2)$$

Continuity

$$\frac{\partial \bar{\eta}}{\partial t} + \frac{\partial}{\partial x}\ (Ud) + \frac{\partial}{\partial y}\ (Vd) = 0 \tag{3}$$

Here g is the acceleration due to gravity, ρ is the mass density of water, d is the total depth = $h + \bar{\eta}$, h being the local still water depth, τ_{bx} and τ_{by} are the bottom friction stresses in the x and y directions, respectively, S_{xx} , S_{xy} , and S_{yy} are radiation stresses (refer to Longuet-Higgins and Stewart (7) for their significance), and τ_{xy} is the lateral shear stress due to turbulence. For monochromatic waves, the radiation stresses are defined in terms of the local values of the wave height H , wave number k , and wave direction θ . For the numerical model under consideration, the latter variables are obtained by using a considerably modified form of the refraction program developed by Noda, et al. (9). This particular program has the advantage that H , k , and $\bar{\theta}$ can be computed at the centers of the cells of a rectangular numerical grid, and wave breaking can be accounted for by a breaking index model for wave heights in the surf zone. Wave-current interactions may also be taken into account; however, this last feature was not used in the results that follow.

Bottom Friction. For the bottom friction, a linear formulation, similar to that of Longuet-Higgins (8), was used for the applications that are described here. Thus,

$$\tau_{bx} = \rho\ c\ <|u_{orb}|>\ U \tag{4}$$

$$\tau_{by} = \rho\ c\ <|u_{orb}|>\ V \tag{5}$$

where c is a drag coefficient (of the order of 0.01) and $<|u_{orb}|>$ is the time average, over one wave period, of the absolute value of the wave orbital velocity. From linear wave theory,

a. CROSS-SECTION A-A
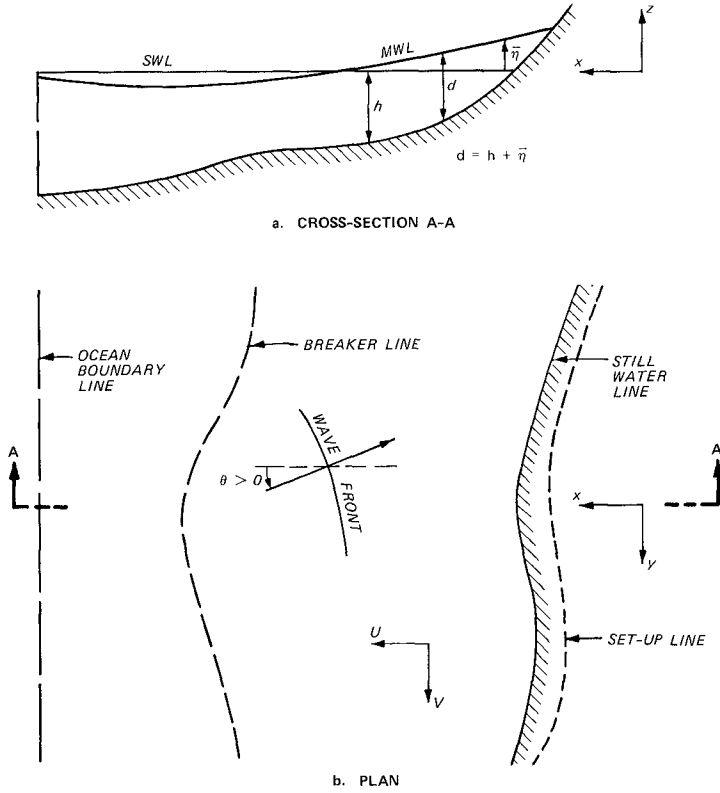
b. PLAN

Figure 1.   Definition sketch for an irregular beach

$$< \left| u_{orb} \right| > \; = \; \frac{2H}{T \; \sinh \; kh} \tag{6}$$

where T is the wave period. Eqs. 4 and 5 amount to a "weak current" assumption. The numerical model described here has the flexibility that other formulations such as a non-linear friction can be easily incorporated in the future.

Lateral Shear. In the numerical model, the coordinate scheme was chosen such that x was positive offshore and y was in the alongshore direction. An eddy viscosity formulation was chosen for the lateral shear, τ_{xy}. The eddy viscosity was assumed to be non-isotropic. Denoting ε_x and ε_y as the eddy viscosities in x and y directions, respectively, in general, ε_y was assumed to be a constant and ε_x a function of x and y. Accordingly,

$$\tau_{xy} = \rho \; (\varepsilon_y \; \frac{\partial U}{\partial y} + \varepsilon_x \; \frac{\partial V}{\partial x}) \tag{7}$$

For the plane beach application with lateral mixing, the eddy viscosity ε_x was assumed to vary within the surf zone in the manner suggested by Longuet-Higgins (8):

$$\varepsilon_x = N \; x \; \sqrt{gh} \tag{8}$$

where x is the distance from the shoreline and N is an empirical coefficient. The eddy viscosity was kept constant beyond the breaker line.

For the field application, the eddy viscosity ε_x was chosen according to the relationship given by Jonsson, et al. (6). Thus,

$$\varepsilon_x = \frac{H^2 gT}{4\pi^2 h} \; \cos^2 \theta \tag{9}$$

This represents twice the value used by Thornton (12). It was felt that Eq. 9 represented the eddy viscosity values for the field situation more realistically than Eq. 8.

Numerical Model

Numerical Scheme. The numerical current model uses a three time level, alternating direction, implicit, finite difference scheme. The model is based on a long wave model known as WIFM (Waterways Experiment Station (WES) Implicit Flooding Model) (refer to Butler (3) for details). In view of the similarity between the equations for long waves and currents, WIFM was converted into a model for currents by the addition of radiation stress terms and modification of friction and eddy viscosity terms, etc. Because of the advection terms, a stabilizing correction

scheme was used. The numerical model has the capability that the size of the grid cells in both horizontal directions may be varied so that the grid may be made finer in regions of greater interest such as the surf zone, inlets, etc. For this purpose, a mapping function defining the mapping from real (X) space to the computational (α) space is used. The function is

$$X_i = a_i + b_i \, \alpha_i^{c_i} \qquad\qquad i = 1,2 \qquad\qquad (10)$$

where X_1, X_2 correspond to x and y, respectively, and the coefficients a_i, b_i, and c_i are calculated for different regions of the grid by an interactive program. The mapping transforms the variable grid in real space to a uniform grid in computational space. Afterwards, the relevant equations are solved in the computational space.

Solution Technique. In order to apply the finite difference scheme, a rectangular grid is used to represent the region of interest. In real space, the cell dimensions in x and y directions are denoted by Δx and Δy. These dimensions may vary from cell to cell. This grid is mapped into a uniform grid with constant cell dimensions $\Delta\alpha_1$ and $\Delta\alpha_2$ in the computational space. Let m and n denote indices in the x and y directions corresponding to the center of an arbitrary cell (refer to Fig. 2). All the variables except the velocities U and V are defined at the cell centers. Velocities U and V are defined respectively at cell faces $m + 1/2$ and $n + 1/2$. The time level is indicated by a superscript k. The governing equations are written in a finite difference form. To advance the solution from a time level k to $k + 1$, an intermediate stage of the solution marked by a superscript * is introduced. The solution procedure is carried out in a two-step operation. In the first step, we sweep the grid in the x-direction. The x-momentum equation is centered about the cell face $m + 1/2$ and the continuity equation about the center of the cell (m,n) and the two equations are solved, using in the process the result $U* = U^{k+1}$. At the end of this sweep, we know $\bar{\eta}*$ and U^{k+1}. Next we sweep the grid in the y-direction. In this sweep, the y-momentum equation is centered about the cell face $n + 1/2$ and the continuity equation about the cell center (m,n). Upon solving the two equations, the values $\bar{\eta}^{k+1}$ and V^{k+1} for each cell are obtained. Thus the two sweeps together complete the solution.

For each sweep, the governing equations for all the cells together with the boundary conditions can be arranged in the form of a matrix equation involving the unknown variables. Since the matrix is tridiagonal, the solution is obtained by recursion. Finally, it should be emphasized that even though we have discussed the solution procedure in terms of (x, y) coordinates for convenience, actually the governing equations are first transformed into the (α_1, α_2) coordinate scheme and solved in the computational space.
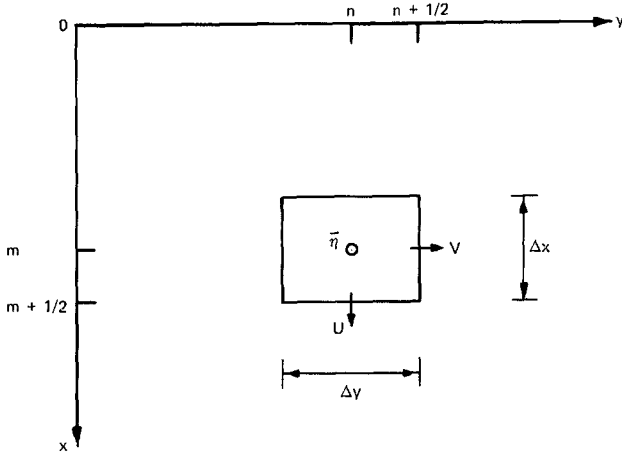
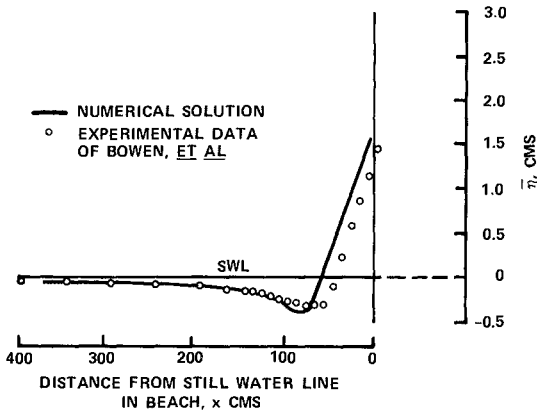Figure 2.   Notation for a cell

Figure 3.   Comparison of the numerical solution for set-up with
            experimental data

Initial and Boundary Conditions. In order to solve the problem
under consideration, appropriate initial and boundary conditions must be
applied. For the examples reported here, an initial condition of rest
was chosen so that $\bar{\eta}$, U and V are zero at the start of the calculations.
To avoid shock, the radiation stress gradients were gradually built up
to their full values over a number of time steps. The solution was
stopped when a steady state was reached.

As for boundary conditions, along the shoreline a 'no flow' (wall)
condition was assumed at the still water line. Thus, no flooding was
permitted on the beach. For the lateral boundaries, a flux type boundary
condition was often used. That is, the flux at a boundary cell was made
equal to that at the next interior cell. It worked very well. For the
offshore boundary, it is common practice to use conditions of either 'no
flow' (wall) or constant elevation. However, both of these are highly
reflective in nature and as a result the transients developed during the
start-up of the numerical solution tend to bounce back and forth between
the offshore and nearshore boundaries and take a long time to damp out.
This is highly undesirable. In view of this, a radiation boundary
condition of the type suggested by Orlanski (11) was selected for the
offshore boundary and implemented in the numerical scheme. It worked
quite well and permitted the transients to propagate out of the grid and
allowed the set-down at the offshore boundary to assume an appropriate
value.

Tests for Idealized Conditions

To develop confidence in the validity of the model and the accuracy
of its results, several tests were run on the model and comparisons were
made between model results and available laboratory data and analytic
solutions. All of these tests were for plane beaches, for which the
coordinate scheme is chosen such that the y-axis coincides with the
still water line in beach and the x-coordinate is measured from the
still water line. Note that for plane beaches, there is no variation
in the alongshore (y) direction.

Plane Beach: Normal Incidence. The model was run for a case of
normal incidence on a plane smooth laboratory beach, reported by Bowen,
et al. (1). The conditions were as follows: T = 1.14 sec, deep water
wave height H_o = 6.45 cm, and beach slope s = 1:12. To run this case on
the model, a 50 x 3 variable rectangular grid with overall dimensions of
approximately 40 m x 30 cm (the laboratory channel was 40 m long) was
used with $\Delta\alpha_1 = \Delta\alpha_2$ = 10 cm and Δt = 0.05 sec. In this example, walls
were used for the lateral boundaries as well as the offshore boundary to
correspond to the laboratory situation. Since for normal incidence, the
velocities U and V would be zero everywhere corresponding to the
steady state, advection, eddy viscosity and friction terms were turned
off in the model. The solution allowed for the effect of set-up on the
wave heights in the surf zone. As the solution proceeded, since $\bar{\eta}$
changed, the wave heights for cells in the surf zone were computed
afresh for each time step by using $H = \gamma(h + \bar{\eta})$, where γ is a
breaking index and the radiation stresses were changed accordingly. As

suggested by Bowen, et al., a γ of 1.15 was used. A build-up time of
10 Δt was used at the start. A comparison of the steady-state set-up
values from the model (after 150 Δt) with those observed by Bowen, et al.
is shown in Fig. 3. As can be seen, there is excellent agreement in the
offshore region. In the surf zone, the numerical model predicts higher
set-ups than observed. This is not surprising since the model does not
allow flooding and runup. It is to be noted that the slope of the mean
water line in the surf zone is approximately the same in both cases.

    Plane Beach: Oblique Incidence. For this case, a plane beach of
constant bottom slope s = 1:30 was selected. A monochromatic wave with
the following deep water characteristics was chosen: T = 12 sec,
H_o = 10 ft, and angle of incidence in deep water, θ_∞ = 20 deg. A drag
coefficient c of 0.01 and a breaking index γ of 0.82 were used in the
model. A 100 x 6 uniform grid with $\Delta x = \Delta y$ = 60 ft was used for most of
the runs. Uniform flux and radiation boundary conditions were used for
the lateral and offshore boundaries, respectively. The build-up time
varied from 15 Δt to 50 Δt, depending on the Δt used.

    First the model was run without allowing for the effect of set-up
on wave heights and radiation stresses. Mixing and advection were
ignored. A time step Δt of 0.5 sec was used. The steady-state velocity
distribution obtained (after 800 Δt) is compared to the triangular dis-
tribution of Longuet-Higgins in Fig. 4. There is good agreement. Note
that for positive θ , V will be negative for our coordinate scheme.
Later a finer grid ($\Delta x = \Delta y$ = 30 ft) with a Δt of 0.25 sec was used. As
can be seen in Fig. 4, as the grid is made finer, the numerical solution
tends to approach the analytic solution.

    The effect of set-up was taken into account next. A time step Δt
of 1.5 sec was used for this case. The velocity distribution from the
model is compared to the corresponding analytic solution in Fig. 5.
There is good agreement. Note that the numerical solution goes to zero
at the still water line because a wall was assumed there. On the other
hand, Longuet-Higgins' solution goes to zero at the set-up line. To
plot his solution, the distance from the still water line to the set-up
line was estimated by using a relation provided by Dalrymple, et al.
(4).

    The effect of lateral mixing was studied next, without taking the
effect of set-up into account. A time step Δt of 5.0 sec was used for
these runs. The mixing parameter P of Longuet-Higgins was varied
between 0.01 and 0.4. Note that P is defined as

$$P = \frac{\pi}{\gamma} \frac{sN}{c} \qquad\qquad (11)$$

Fig. 6 shows the effect of P on the numerical solution. As expected,
the magnitude of the peak decreases, the peak moves closer to the shore-
line and the velocities offshore of the breaker line increase as P
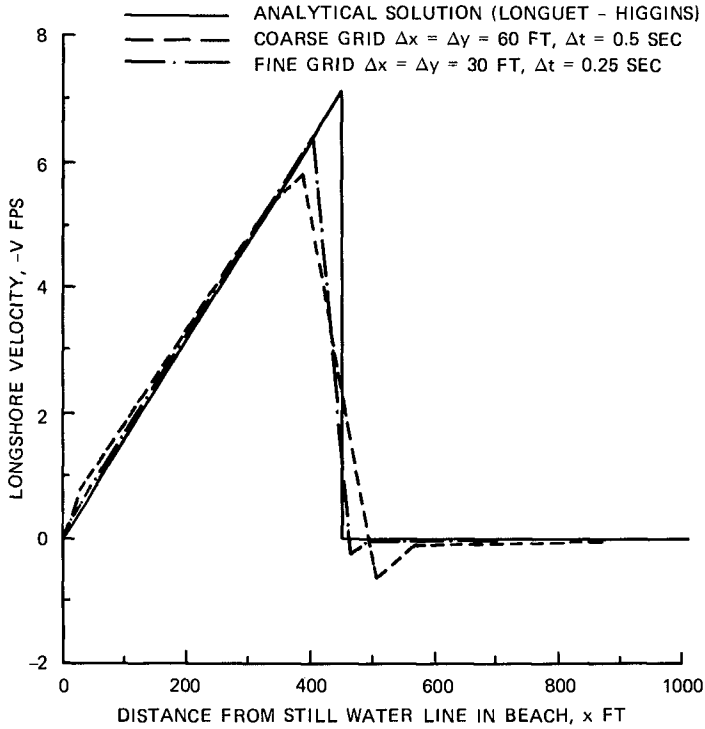increases.

Figure 4. Plane Beach: Solution for longshore current without
           taking set-up into account
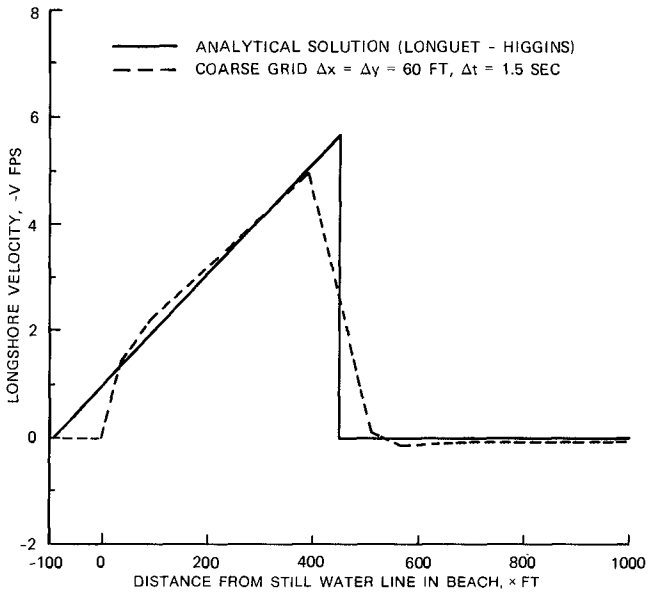
Figure 5.   Plane Beach: Solution for longshore current taking
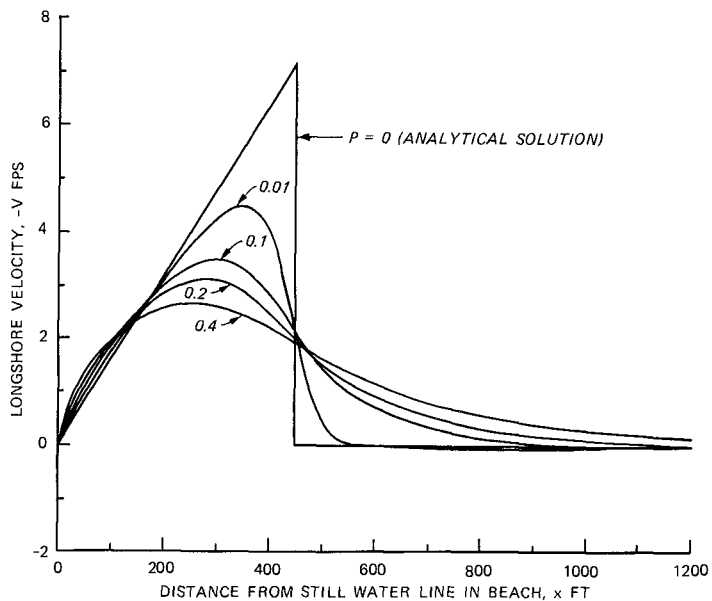   set-up into account

Figure 6. Plane Beach: Effect of mixing parameter P on the numerical solution (set-up is neglected)

Difficulties Involved in Applications to Field Situations

    While it is relatively easy to apply a numerical current model to
idealized cases, one must face several difficulties in applying the
model to field situations. Among these is the highly irregular nature
of the bathymetry, especially near inlets where channels and shoals
exist. The topography must be smoothed to a certain extent in order for
the wave climate and longshore current models to work properly. Yet,
one must be careful not to completely change the basic features of the
topography. The shoreline as well as the breaker line may be irregular
and may be oblique to the grid axes. There may be more than one breaker
line. There are problems connected with discretization of the shoreline
and breaker line(s). Selection of appropriate values for empirical
coefficients such as friction and eddy viscosity coefficients and
breaking index is not easy. There are problems in connection with the
wave climate model also, especially if wave-current interactions are to
be taken into account.

A Particular Field Application

    In order to demonstrate the applicability of the numerical model to
field situations, the case of Oregon Inlet, North Carolina, was selected.
Oregon Inlet is a tidal inlet in a barrier island system. Behind the
inlet toward the main land is Pamlico Sound. Most of the problems
mentioned in the previous paragraph had to be addressed and solved
satisfactorily in this application. For purposes of the numerical
simulation, a rectangular region approximately 62,400-ft long in the
alongshore direction and 29,400-ft wide in the offshore direction was
considered. It included a portion of Pamlico Sound. The variable grid
used for the simulation is shown in Fig. 7. The grid was 77 cells wide
in the alongshore direction and 54 cells wide in the offshore direction.
It may be noted that the minimum cell widths in the alongshore and
offshore directions were 400 and 100 ft, respectively. These widths
were used near the inlet and surf zone, respectively. Note that $\Delta\alpha_1 =$
$\Delta\alpha_2 = 100$ ft. The topography used in the simulation corresponding to
this grid is shown in Fig. 8. The elevations are shown in feet and the
datum is Mean Low Water (MLW). There are several points that must be
mentioned about this three-dimensional perspective plot. First, the
vertical dimensions are highly exaggerated compared with the horizontal.
Secondly, the depths are plotted in the computational space and not the
physical space. So the horizontal dimensions are distorted. The
topography was somewhat modified compared to the actual topography, with
respect to the depths near the offshore boundary and the land elevations
on the islands. In spite of these factors, Fig. 8 helps one to visualize
the irregular nature of the bathymetry. Also, the locations of the
channels and shoals in the region of the inlet may be seen clearly in
the figure.

    A monochromatic wave with a height of 11.39 ft, period of 8.0 sec,
and $\theta = 51.1$ deg in 60-ft depth of water was selected for the simulation
(the depth of water at the offshore boundary of the numerical grid was
60 ft). This wave corresponded to the significant wave during a part of
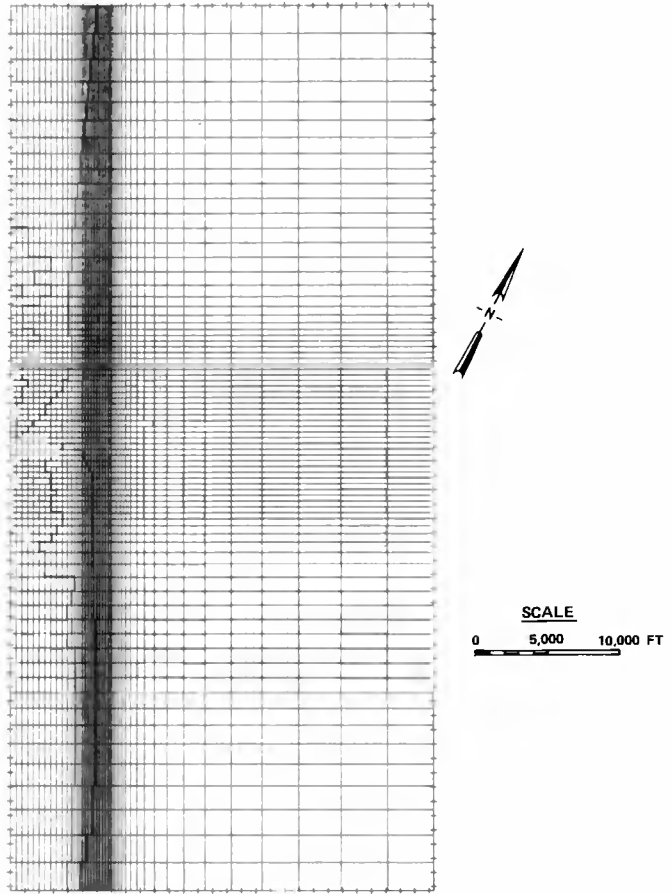the Ash Wednesday storm of March 1962 at the inlet. In this case,

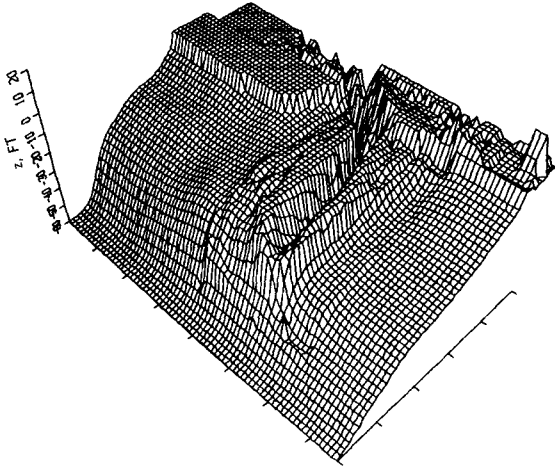Figure 7.   Numerical grid for Oregon Inlet, North Carolina

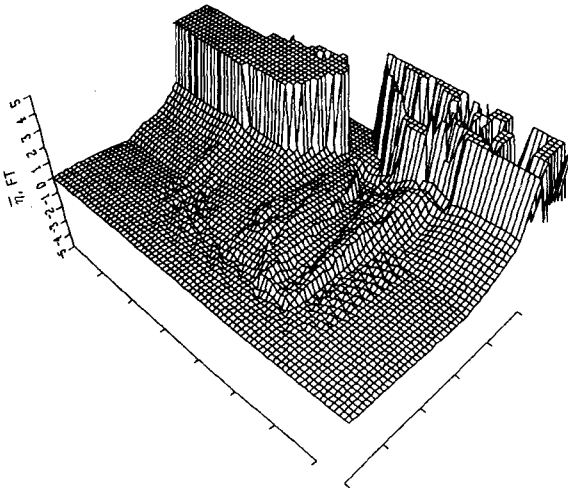Figure 8.   Topography for Oregon Inlet Numerical Model

Figure 9.   Surface elevation plot for Oregon Inlet

besides using 'no flow' conditions at the shoreline, a radiation boundary
condition offshore and flux boundary conditions at the lateral boundaries,
a flux boundary condition was used over a part of the inland side of the
Sound, while the rest of the Sound was closed off. A time step Δt of
18.0 sec and a drag coefficient c of 0.01 were used in the numerical
model. The breaking index γ was chosen according to the breaking
criterion employed by Noda (10):

$$\frac{H_b}{L_b} \approx 0.12 \tanh \left(\frac{2\pi d_b}{L_b}\right) \tag{12}$$

where L corresponds to the wave length and the subscript b indicates
values at breaking. A build-up time of 15 Δt was used at the start.
The eddy vicosity ε_x was chosen according to Eq. 9 and the eddy vis-
cosity ε_y was set equal to the value of ε_x at the offshore boundary.
For the case under consideration, the complete equations (Eqs. 1, 2, and
3) were solved. An approximate steady-state was reached after 67 Δt.
Figs. 9 and 10 represent the corresponding mean water levels and veloc-
ity vectors, plotted on the grid in the computational space. The veloc-
ity vectors are plotted for every other cell in each coordinate direction.
To avoid confusion, the plotting of velocities with mangitudes less than
0.1 ft/sec is suppressed.

Referring to Figs. 8, 9, and 10, let us first consider the two
portions of the beach away from the inlet. The shorelines in these
regions are approximately straight and the contours are approximately
straight and parallel. As we approach the shoreline from offshore,
there is a small set-down followed by a set-up. The velocities are
mainly alongshore and the velocity distribution is similar to that for
a plane beach except that it exhibits two peaks at some locations.

The situation is more complicated in the region of the inlet (the
central part of the grid). Here the breaker line is farther offshore.
The depth in the main channel decreases first and increases later as we
go toward the inlet. Because of these factors, the water sets up around
the inlet and tends to create a flow into the inlet through the various
channels, as one would naturally expect. A part of the main alongshore
flow goes around the channels and shoals, to the other side.

Near the shoals, the patterns of mean water level and velocity are
irregular. This is because of the fact that the waves refract around
the shoals and break, creating locally set-ups and currents that do not
necessarily conform to the general patterns. As the waves go toward the
islands, they re-form because the depth increases.

Figs. 9 and 10 do not reflect the influence of tides and freshwater
flows through the inlet. In nature, these phenomena tend to modify the
patterns shown in these figures.

Computational Costs. For those interested in computational times,
it should be noted that all the computations described in this paper
were performed on a Cray-1 computer, which has vectorizing capabilities.
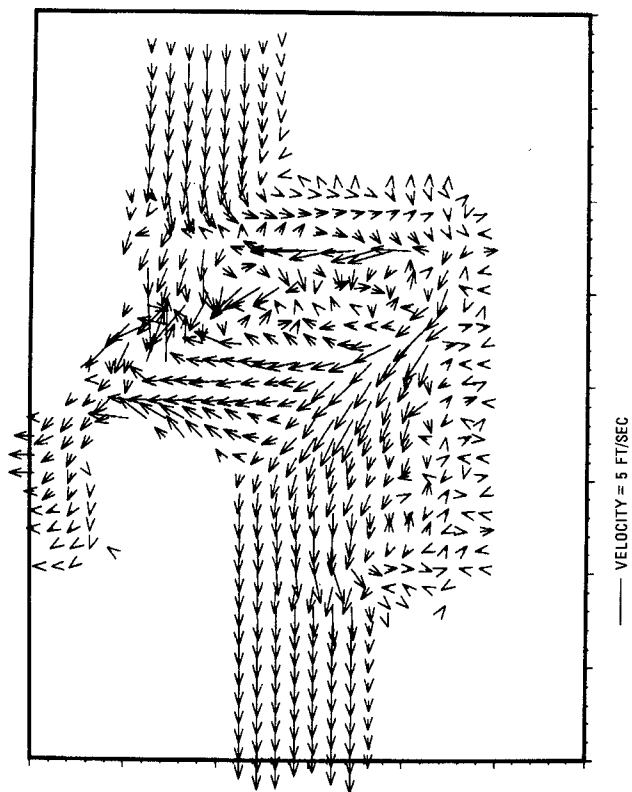
VELOCITY = 5 FT/SEC

Figure 10. Velocity vector plot for Oregon Inlet

For the field application involving a 54 x 77 grid with 4,158 grid points, the Central Processor Unit (CPU) time for 67 time steps of simulation was approximately 15.5 seconds. The total cost for the job including program compilation, CPU time and data file manipulation, was approximately ten U. S. dollars. So the computational costs for the model may be considered reasonable.

Conclusions

A generalized longshore current model was developed. It retains the unsteady terms as well as advection and lateral mixing terms in the equations of motion and can be easily modified for different formulations of friction, eddy viscosity, etc.

A radiation boundary condition was successfully applied to the offshore boundary. It permits the transients due to start-up of the numerical scheme to be propagated out of the numerical grid.

Comparisons were made with known analytic solutions and experimental results. There was good agreement.

The model was applied to a complex field situation and the results obtained appeared to be reasonable. The computational costs were modest.

For the future, it is proposed to allow non-linear friction. Coordinate transformations will be used to transform the shoreline and breaker line(s) into lines parallel to the coordinate axes. It is proposed to simulate also the effect of structures such as jetties on the longshore currents and nearshore circulation.

Acknowledgements

References

1. Bowen, A. J., Inman, D. L., and Simmons, V. P., "Wave 'Set-Down' and Set-Up," Journal of Geophysical Research, Vol. 73, No. 8, 1968, pp. 2569-2577.

2. Bowen, A. J., "The Generation of Longshore Currents on a Plane Beach," Journal of Marine Research, Vol. 27, 1969, pp. 206-215.

3. Butler, H. L., "Evolution of a Numerical Model for Simulating Long Period Wave Behavior in Ocean-Estuarine Systems," Estuarine and Wetlands Processes with Emphasis on Modeling, Marine Science Series, Vol. 11, Plenum Press, New York, 1980.

4. Dalrymple, R. A., Eubanks, R. A., and Birkemeier, W. A., "Wave-Induced Circulation in Shallow Basins," Proceedings, Journal of the Waterway, Port, Coastal and Ocean Division, ASCE, Vol. 103, No. WW1, February 1977, pp. 117-135.

5. Ebersole, B. A., and Dalrymple, R. A., "Numerical Modelling of Nearshore Circulation," Proceedings, 17th Conference on Coastal Engineering, 1980, Vol. III, Chapter 163, pp. 2710-2725.

6. Jonsson, I. G., Skovgaard, O., and Jacobsen, T. S., "Computation of Longshore Currents," Proceedings, 14th Conference on Coastal Engineering, 1974, Vol. II, Chapter 40, pp. 699-714.

7. Longuet-Higgins, M. S., and Stewart, R. W., "Radiation Stresses in Water Waves; A Physical Discussion, with Applications," Deep-Sea Research, Vol. 11, 1964, pp. 529-562.

8. Longuet-Higgins, M. S., "Longshore Currents Generated by Obliquely Incident Sea Waves, 1 and 2," Journal of Geophysical Research, Vol. 75, No. 33, November 1970, pp. 6778-6789 and pp. 6790-6801.

9. Noda, E. K., Sonu, C. J., Rupert, V. C., and Collins, J. I., "Near-shore Circulations Under Sea Breeze Conditions and Wave-Current Interactions in the Surf Zone," Tetra Tech Report TC-149-4, February 1974.

10. Noda, E. K., "Wave-Induced Nearshore Circulation," Journal of Geophysical Research, Vol. 79, No. 27, September 1974, pp. 4097-4106.

11. Orlanski, I., "A Simple Boundary Condition for Unbounded Hyperbolic Flows," Journal of Computational Physics, Vol. 21, 1976, pp. 251-269.

12. Thornton, E. B., "Variation of Longshore Current Across the Surf Zone," Proceedings, 12th Conference on Coastal Engineering, 1970, Vol. I, Chapter 18, pp. 291-308.

13. Vreugdenhil, C. B., "A Method of Computation for Unsteady Wave-Driven Coastal Currents," Report R 1174, Part I, Waterloopkundig Laboratorium, Delft Hydraulics Laboratory, August 1980.